Honors Thesis

RESOLVING PSEUDOSYMMETRY IN γ-TIAL USING CROSS-CORRELATION ELECTRON BACKSCATTER DIFFRACTION WITH DYNAMICALLY SIMULATED REFERENCE PATTERNS

by

Brian Jackson

Submitted to Brigham Young University in partial fulfillment of graduation requirements for University Honors

Mechanical Engineering Department

Brigham Young University

April 2017

Advisor: David Fullwood

Honors Coordinator: Brian Jensen

ABSTRACT

RESOLVING PSEUDOSYMMETRY IN γ-TIAL USING CROSS-CORRELATION ELECTRON BACKSCATTER DIFFRACTION WITH DYNAMICALLY SIMULATED REFERENCE PATTERNS

Brian Jackson

Mechanical Engineering Department

Bachelor of Science

Pseudosymmetry is a phenomenon that occurs in EBSD when grains with different lattice parameters produce nearly identical diffraction patterns such that conventional EBSD techniques are unable to unambiguously differentiate the lattice orientations. This commonly occurs in materials with near-unity tetragonality, such as γ-TiAl. The current study uses cross-correlation EBSD ("CC-EBSD", or "HR-EBSD") to resolve pseudosymmetry in γ-TiAl. Three dynamically simulated reference patterns are generated for each point in the scan, one for each of the three potential pseudosymmetric orientations, which are subsequently correlated with the original pattern using six different methods in order to identify the correct orientation. The methods are first applied to a scan of dynamically simulated patterns, which is used to evaluate the sensitivity of the method to pattern resolution, pattern noise, and pattern center error. After determining that all six methods were 100% successful up to about 13 μm of pattern center error and pattern resolutions of about 80x80 pixels, the methods were applied to an experimental sample of lamellar γ-TiAl. A hybrid combination of two of the methods was shown to successfully pick the correct pseudosymmetric for about 96% of the points in the scan, improving upon the 70% accuracy of the Hough-based methods for the current study, and 90% accuracy for previous studies resolving pseudosymmetry in lamellar γ-TiAl.

ACKNOWLEDGEMENTS

I would like to acknowledge the help and support of my advisor, Dr. David Fullwood, who helped me throughout the entire process. I also acknowledge the help of Stuart Wright at EDAX who helped throughout various stages of the research, as well as Jordan Christensen, who helped with the sample preparation and data collection. The research was supported by the U.S. Department of Energy (DOE), Office of Science, Basic Energy Sciences (BES), under Award #DE-SC0012587.

TABLE OF CONTENTS

LIST OF FIGURES

LIST OF TABLES

1 Introduction

Electron backscatter diffraction (EBSD) is a common method of analyzing the microstructure of materials composed of crystalline lattices. By bombarding a material sample with an electron beam, diffracted electrons that exit the sample surface are intercepted by a screen. The resulting electron backscatter diffraction pattern (EBSP), captured using a low-light camera, can be analyzed to obtain information about the crystal structure and orientation. By scanning areas of the sample and collecting EBSPs at multiple locations, the orientation information obtained from EBSP analysis can be used to identify grains in polycrystalline materials, analyze grain boundary characteristics, and perform texture analysis [1], [2]. Traditional EBSP analysis techniques utilize Hough transforms to identify band positions. The Hough transform maps a line in an image to an intercept and angle on a scatter plot; EBSD bands are transformed to "Hough peaks" in Hough space that are then used to determine the orientation of the crystal based upon a specified lattice structure; this process is often referred to as "indexing." Automated methods for indexing EBSPs are commonly used, generally via software that directly controls the scanning electron microscope (SEM) used to collect the patterns. Precision of the orientation determination is typically some fraction of a degree [3]–[5].

Currently, automated Hough-based indexing algorithms have difficulty resolving pseudosymmetry [6]–[11]. Pseudosymmetry occurs when two patterns have nearly identical band positioning, but unique crystallographic orientations, as shown in Figure 1, where, to the naked eye, the patterns appear identical, but have subtle differences that need to be resolved. Pseudosymmetry is commonly found in materials with a near-cubic lattice structure where one of the three principal axes is slightly longer than the other two. Tetragonality is the measurement of relative elongation of the longer axis and is defined according to the following formula [12]:

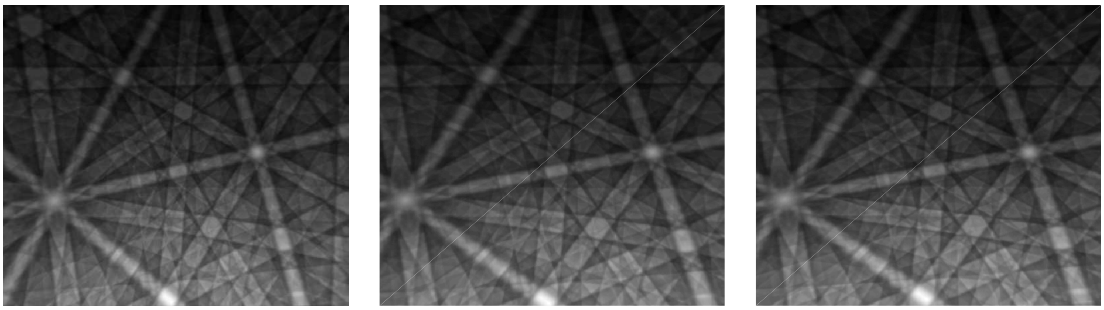

Figure 1: Simulated EBSP's of three pseudosymmetric lattices of γ-TiAl

$$\epsilon^{tet} = c - \frac{a+b}{2} \tag{1}$$

where a, b, and c are the lattice constants.

Titanium aluminides (commonly used in commercial aero-engines), martensite (an extremely hard phase of steel), and lead zirconate titanate (PZT), are common engineering materials with a tetragonal lattice structure that exhibit pseudosymmetry. In γ-TiAl, for instance, the ratio c/a is usually about 1.02. Resolution of pseudosymmetric orientations in these materials is important in identifying the slip systems that uniquely contribute to their strength and hardening characteristics.

Several approaches have been used to resolve pseudosymmetry. Zambaldi et al [6] proposed using a fit characteristic of the indexing algorithm—or the angular deviation between the measured and expected Hough peak vectors—to correctly identify orientations in pseudosymmetric materials. This approach achieved a successful indexing rate up to 90% in a sample of lamellar γ-TiAl. Other recent approaches have used more recent high-resolution, or cross-correlation, EBSD techniques to attempt to resolve pseudosymmetry [7], [13].

High-resolution EBSD (HR-EBSD), or cross correlation EBSD (CC-EBSD), extends the precision of traditional Hough methods by correlating deformations of the pattern with deformations of the lattice in all three dimensions. The shifts required to align the two regions are calculated using the convolution of many sub-regions

of the patterns through the use of Fast Fourier Transforms (FFT). The combined effect of these shifts are then used to calculate the relative distortion and disorientation between the two patterns. This technique offers excellent relative orientation determination, several orders of magnitude better than Hough techniques [14]–[16]. Although CC-EBSD is typically applied to the measurement of strain between patterns, the current paper will be applying the same technique to detect subtle differences between pseudosymmetric patterns. Essentially, even when two strain-free patterns match closely but not perfectly, the deformation between them and their "pseudostrain" will be small, whereas patterns that do not match will have a larger relative deformation and "pseudostrain." The ability of CC-EBSD to capture and quantify minute differences between patterns is the basis for its application to resolving pseudosymmetries.

Within the CC-EBSD technique exist two fundamental approaches for selecting the reference pattern: selecting an experimental pattern or generating a simulated pattern. The traditional method selects a pattern from the same grain as the pattern of interest, typically from a centralized location in the grain that is expected to have the lowest distortion [15]. One reason for more extensive use of experimental, or "real," reference patterns (as opposed to simulated reference patterns) is due to the difficulty of accurately determining microscope geometry for replication in the simulated patterns [17], [18]. Since a real reference pattern comes from the same microscope arrangement, typical uncertainty in microscope geometry can be tolerated in the determination of relative distortion. However, because the absolute orientation of the reference pattern is not necessarily known, the ability to resolve pseudosymmetric patterns is limited.

The second reference pattern approach consists of generating a simulated reference pattern. Since the distortion and orientation of the simulated pattern are precisely known, the relative distortion and orientation information generated by the

cross-correlation approach can theoretically determine the absolute distortion and orientation of the experimental pattern. The determination of absolute distortion allows for the calculation of absolute strain and therefore tetragonality, which can be used to resolve pseudosymmetric orientations based upon the identification of the elongated tetragonal axis, or c-axis.

Furthermore, if a quantitative measure of tetragonality is not required, several methods exist within HR-EBSD to calculate a quantitative measure of fit, or correlation, between the experimental pattern and reference patterns that reflect different pseudosymmetric options. Although pseudosymmetric orientations have nearly identical band positions, their band intensity profiles—composed of band intensities and band widths—are unique, such that they can often be resolved by magnified visual inspection [6]. Hence a pixel-by-pixel comparison of correlation between the experimental and reference images may adequately resolve pseudosymmetry [7].

There are currently two principal methodologies used to generate simulated EBSPs: kinematical simulation and dynamical simulation. Kinematical simulations are simplistic simulations based upon Bragg's Law; this approach defines positions for which constructive interference of scattered electrons occurs, from lattice planes of a specified interplanar spacing. Kinematical simulations accurately replicate band positions, but they suffer from poor band profile and intensity replication, especially near band axes. However, due to the simplistic nature of the simulation, they can be generated very quickly using efficient algorithms, typically in under a second [16], [19], [20]. Dynamical simulations, on the other hand, are based upon a Monte Carlo simulation which computes the trajectories of individual electrons as they interact with the crystal and undergo scattering events [21], [22]. By simulating the trajectories of several million electrons, a high-fidelity EBSP can be generated that accurately replicates band position, profile, and intensity [23]. The Monte Carlo simulation is extremely computationally intensive, taking anywhere from 6-30 minutes, depending

upon the type of graphics card available [24], or hours for lower symmetry materials; however, once the initial "master" EBSD pattern is generated by the Monte Carlo simulation, patterns for individual orientations of the material can be quickly generated ($<$ 1 second). Since accurate simulation of band profiles are likely very important in resolving pseudosymmetry, and dynamically simulated patterns have been shown to be both more accurate and precise than kinematically simulated patterns at low levels of relative strain between the experimental and reference patterns [24], dynamically simulated patterns were considered the better option for resolving pseudosymmetry in this study.

As briefly discussed above, accurate determination of microscope geometry presents a significant challenge when using simulated reference patterns. The pattern center of an EBSP, defined as the location where the electrons impinge normal to the surface of the detector screen, can have a significant effect on the calculation of absolute strain and tetragonality. If the assumed pattern center is incorrect, the reference pattern will be slightly shifted relative to the experimental pattern, resulting in artificial differences between the two patterns. Since pseudosymmetric orientations so closely resemble each other, it is imperative that the pattern center error is small, otherwise an incorrect orientation may be selected as the correct one. The sensitivity of the above methodologies to pattern center error is analyzed, and methods for minimizing the influence of pattern center error on resolution of pseudosymmetry are assessed.

Furthermore, it is also desirable to know how sensitive the methodology is to poor pattern quality. Several factors can affect pattern quality, including poor sample polish, internal structural entropy, electronic and detector noise, or low electron yield. Current methods for resolving pseudosymmetry, such as superlattice reflection detection using EBSD with long exposure times and high acceleration voltages or TEM analysis, are dependent upon extremely careful sample preparation and laborious or time-insensitive measurement processes [6], [8]. Therefore, if the current methodology

is able to work with sub-optimal patterns, it will be advantageous over other more exacting methods.

In summary, the purpose of the current paper is to expand upon previous studies investigating the effectiveness of using cross-correlation EBSD with dynamically simulated reference patterns to discern subtle differences between pseudosymmetric orientations in order to correctly identify the lattice orientation. Several potential methods for discerning these differences, including both CC-EBSD techniques as well as holistic pattern comparison techniques, will be used in an attempt to resolve pseudosymmetry in a common engineering material. Additionally, the effects of pattern center error, pattern resolution, and pattern quality on the accuracy of this resolution will be evaluated.

2 Methods

2.1 Material Samples

The current study used γ-TiAl to evaluate the effectiveness of HR-EBSD with dynamically simulated reference pattern in resolving pseudosymmetry. Due to its low density, nearly constant yield strength up to 1073 K, and good corrosion and creep resistance, γ-TiAl is an excellent choice of material in high-temperature structural components, such as in jet engines and turbines. The structure of the γ-TiAl phase is a face-centered-cubic-derived tetragonal lattice. The c-axis is about 2% longer than the a-axis due to alternating layers of titanium and aluminum occupying the (002) planes. This results in 3 pseudosymmetric orientations, all separated by successive 120 degree rotations about the (111) plane normal. For a detailed description of orientation variants and domain structure of γ-TiAl refer to [6].

The ability to resolve pseudosymmetry, and thus better characterize the detailed

microstructure, will aid the understanding of deformation modes and related strength and hardening characteristics in this important engineering material. Additionally, γ-TiAl was selected as an appropriate material for this study given the existing literature dealing with γ-TiAl and its pseudosymmetric variants [6]–[11].

Both a simulated and an experimental scan of EBSPs were created as testbeds for the different pseudosymmetry resolution methods. In the case of the simulated scan, the pseudosymmetry is exactly known. For each method, dynamically simulated patterns were correlated with the test scan EBSPs to determine correct lattice orientation, and the effectiveness of the methods were compared.

Simulated Scan

The first step in determining the effectiveness of the proposed methodology involved generating a simulated scan of γ-TiAl. Since the orientation, lattice parameters, and microscope geometry can be exactly specified using simulated patterns, a controlled experiment investigating the ability of dynamically simulated reference patterns to resolve pseudosymmetry could be performed without having to account for variables such as sample preparation, pattern quality, pattern center error, and uncertainty in lattice parameters.

The simulated patterns were generated by EMsoft 3.0, an open-source software package for simulation of electron diffraction and imaging modalities developed at Carnegie Mellon University [25]. As a precursor to generating patterns, a "master" EBSD pattern was formed via the Monte Carlo approach, using the material parameters listed in Table 1, 20 keV accelerating voltage, 70 degree sample tilt, and a resolution of 1024x1024 pixels. All other parameters were set to their default values.

After generating the "master" EBSD pattern, from which any arbitrary orientation can be generated, a series of patterns were created in order to simulate an actual EBSD scan. This simulated scan was designed to consist of 10 grains composed of 10

Figure 2: Orientations of the simulated scan. Each color denotes a set of pseudosymmetric orientations and the different patterns denote a different pseudosymmetry.

patterns each. The orientation within each grain varied by 1 degree over the 10 points within the grain (therefore a 0.1 degree misoriention between neighboring points of the same grain). This was done so that 100 unique orientations were generated, while having easily identifiable sections in the scan. Since pseudosymmetric orientations for γ-TiAl come in trios, three grains were all set to be pseudosymmetric to each other. With 10 grains, 3 sets of pseudosymmetric grains were generated, while the last remaining grain was assigned a random orientation. The orientations were arranged such that one set of pseudosymmetric grains has all three grains adjacent, the other set has two adjacent grains, and the third has all three grains separated (see Figure 2). The adjacency of pseudosymmetric grains was chosen to test dependence of a given pseudosymmetry algorithm accuracy on different transitions between pseudosymmetric orientations. The pattern center was adjusted for each point to match the simulated positions of the scan points. The sample tilt and azimuthal, camera tilt and azimuthal, accelerating voltage, and phosphor screen size were kept at their default values. The scan was replicated along 3 rows so that the indexing software could process the scan.

Lattice Parameters for γ-TiAl

Parameter	Value
a	0.4003 nm
b	0.4003 nm
c	0.4067 nm
Space Group	123
Debye-Waller	0.006 nm^2

Table 1: Lattice parameters for γ-TiAl used by EMsoft and OpenXY

Experimental Scan

A sample of γ-TiAl with a composition of 50% Ti and 50% Al with a lamellar microstructure was prepared by first grinding using 320 grit SiC paper, followed by a 9 micron polycrystalline diamond polish, and polished with 0.05 micron colloidal silica. Following sample preparation the EBSD patterns were collected using an FEI Helios Nanolab 600 SEM with an accelerating voltage of 30 keV, sample tilt of 70 degrees, and a camera elevation of 10 degrees. A 150x151 point scan was taken with a step size of 0.2 μm, resulting in a scan area of about 30x30 μm.

2.2 Sample Analysis

Once the scan was generated, it was indexed using OIM Data Collection 7.2, software developed by EDAX-TSL [26]. It was expected that the indexing would not be able to resolve all of the orientations. The results of the indexing were then analyzed in OpenXY, an open-source software developed by Brigham Young University to perform CC-EBSD analysis using real, kinematically simulated, or dynamically simulated reference patterns [27].

Tetragonality

The first approach to resolving pseudosymmetric orientations in γ-TiAl used OpenXY to calculate the absolute strain of the patterns using dynamically simulated reference patterns. The absolute strain and orientation were calculated using the same iterative methodology used in [16], [20], [24]. As mentioned in the introduction, the CC-EBSD technique converts shifts between the patterns themselves into the overall deformation required to transform one lattice state to the other. When comparing two pseudosymmetric orientations the cross-correlation algorithm will interpret the mis-aligned c-axis as a "pseudostrain" that represents the relative deformation of

one pattern to another, and does not necessarily imply that the lattice itself is in a strained configuration. However, these "pseudostrains" can be used to detect the pseudosymmetric orientation for which the deformation between the lattices is minimal. Measuring the tetragonality of the cross-correlation for each pseudosymmetric orientation is a simple way of reducing the 9-term strain tensor to a single number that can easily be compared.

The first step was to generate a dynamically simulated reference pattern for the orientation given by the indexing software, which was then used to cross-correlate with the experimental pattern using a converging iterative algorithm that generates a new reference pattern based upon the previous cross-correlation. The deformation gradient tensor provided by the cross-correlation algorithm gave an improved estimate of the relative orientation between the two patterns, which was used to generate the reference patterns for the two additional pseudosymmetric orientations by rotating the lattice by 90 degrees about the a-axis and 90 degrees about the b-axis. These patterns were then cross-correlated (without using the iterative algorithm) with the original pattern to determine the deformation gradient tensor between the original pattern and all three of the pseudosymmetric orientations. The tetragonality was calculated for each of the three orientations according to the formula for tetragonality, which is the same calculation as Equation 1 when converted to strain:

$$\epsilon^{tet} = \epsilon_{33}^{crystal} - \frac{\epsilon_{11}^{crystal} + \epsilon_{22}^{crystal}}{2} \tag{2}$$

When the c-axes of the reference and original lattice are aligned, the lattices will be nearly identical so that all relative strain components should be approximately zero. When the c-axes are not aligned, the ϵ_{33} term will decrease, and either ϵ_{11} or ϵ_{22} will increase, resulting in a negative tetragonality. Therefore the non-negative tetragonality should indicate the correct orientation for the original lattice. In the case where the patterns did not align well and there was more than one non-negative

tetragonality, the orientation with the largest positive tetragonality was selected. The method used tetragonal instead of cubic reference patterns in order to more closely approximate the expected lattice geometry. [24] demonstrated that best results are obtained when using dynamical reference patterns with less than a 2% relative tetragonality with the experimental patterns. Since γ-TiAl's 2% tetragonality is on the edge of this limit, tetragonal reference patterns were used to achieve the best possible cross-correlation.

In addition to using tetragonality, other methods were used in an attempt to match the original pattern with the correct pseudosymmetric reference pattern. Using the same 3 psuedosymmetric, dynamically simulated reference patterns generated by OpenXY and EMsoft, several parameters were used and recorded that quantify the correlation between the original pattern and each reference pattern. These include the cross-correlation coefficient, mutual information, shift confidence, and SSE.

Cross-correlation coefficient

The normalized cross-correlation coefficient r is a pixel-by-pixel comparison between two patterns, defined as [28]:

$$r = \frac{1}{n} \sum_{x,y} \frac{(f(x,y) - \bar{f})(t(x,y) - \bar{t})}{\sigma_f \sigma_t} \tag{3}$$

where f and t are the grayscale values of the two patterns, σ_f and σ_t are the standard deviations of the images, and n is the number of points in the images. The coefficient will approach 1 for identical images and 0 for images with zero correlation. In EBSD, it has been used to qualitatively compare the fidelity of simulated patterns by evaluating how close they replicate an experimental image [28].

Mutual information

Mutual information is another method for performing image comparison that has been introduced into the material science community in recent years [29]. This parameter claims to be a more robust method of comparing two images than conventional cross-correlation techniques, so will also be used to attempt to resolve pseudosymmetry. The mutual information is calculated by computing the entropies of the two individual patterns as well as the joint entropy. The individual entropy is calculated by first computing the normalized histogram $p_i = h(i)/N$ of the image, where $h(i)$ is the histogram of image for gray levels between 0 and 255, and N is the number of pixels in the image. The entropy is then defined as $H(A) \equiv -\sum_{i=0}^{255} p_i \ln p_i$. The joint entropy is calculated in a similar manner by first computing the joint histogram $h(i,j)$ of the two patterns, which, when normalized, estimates the probability $p_{ij} \equiv h(i,j)/N$ where N is the number of pixels in the pattern. The entropy is then calculated as $H(A,B) = -\sum_{i,j}^{255} p_{ij} \ln p_{ij}$. The mutual information of images A and B, $I(A,B)$, is then defined as follows [29]:

$$I(A,B) \equiv H(A) + H(B) - H(A,B) \tag{4}$$

Shift confidence

Another potential method of quantifying the quality of the fit between two images is by comparing the sharpness of the peak of the convolution used during the cross-correlation. The convolution of two images results in a peak at the pixel location corresponding to the shift required to align the two images. For similar images, as is typically the case, the convolution is a "hump" with a discrete height and width (see Figure 3). Therefore the magnitude of the peak of the convolution in terms of standard deviations of the entire convolution can be used as an additional measurement of image similarity. For the current study, the shift confidence between

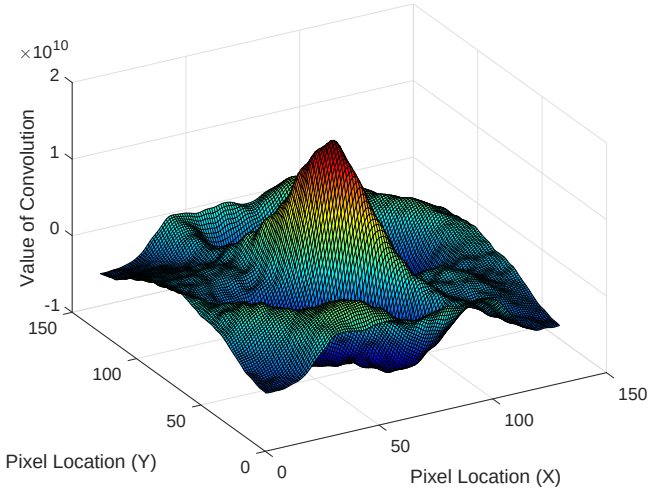

Figure 3: Plot of the convolution of one of the regions of interest for an experimental pattern and represents the shifts between the experimental and the reference patterns. The shift confidence is the height of the peak relative to the rest of the convolution. The horizontal plane is the x and y coordinates of the region of interest, and the height is the value of the convolution at each pixel location

two images, $C(A, B)$, is defined as follows for a convolution of images A and B, $R(A, B)$:

$$C(A, B) \equiv \frac{\max(R(A, B)) - \bar{R}(A, B)}{\sigma_{R(A,B)}} \tag{5}$$

The cross-correlation algorithm selects many sub-regions of the patterns to compare using convolutions. Commonly referred to as regions of interest, or ROI's, the combined shifts of each of these regions is used to calculate the shift of the entire pattern [16], [20], [24]. The shift confidence is also calculated for each of these regions and the average over all of the regions was used to compare each pseudosymmetric orientation. The current study used 48 ROI's arranged in a grid pattern as described in [24].

SSE

The last value used to attempt to quantify the measure the similarity between two images is referred to as the SSE, or sum of squared error, of the cross-correlation. This is calculated as the sum of squares of the lengths of the shifts for each of the ROI's. The SSE of the cross-correlation is simply the norm of the deformation tensor between the two images, which is proportional to the shift required to align the regions of interest; therefore, the more similar the images are, the smaller the shift required to align them and smaller the value of SSE.

Hybrid

It's possible that no single one of previously described methods provides better results in all situations. In cases where relative merits of one methods can identified, a combination of several of the methods, or a hybrid method, may prove to be advantageous in order to combine strengths of different methods to produce a better overall result.

2.3 Pattern Center Calibration

The pattern (or projection) center (PC) calibration is critical for accurate and precise determination of lattice orientation from EBSD and subsequent CC-EBSD analysis. The EBSD system can be calibrated using a variety of methods including a known single crystal [30], shadow-casting [31]–[33], or camera calibration [34]–[36]. In practice, the PC is most often determined using an iterative procedure first proposed by Krieger-Lassen [37] due to its balance of convenience and accuracy.

The PC calibration is performed by first detecting the bands in the pattern either using the Hough Transform or manually locating the bands. The second step is to make an initial estimate of the calibration values (hereafter x^*, y^*, and z^* where x^*

and y^* are the coordinates of the PC in the phosphor screen of the detector and z* is the sample-to-screen distance). When the pattern is indexed using this initial estimate, the bands in the overlay solution should be close enough to those in the experimental pattern that the indexing solution should be able to provide a good enough estimate to start the process. The x^*, y^* and z^* values are then varied, the pattern re-indexed using the same band positions and the orientation re-determined. From the new orientation, the average angular fit [38] between the indexing solution and the detected bands is determined. The fit is the parameter used to judge whether the new pattern center is better than the previous estimate. In the OIM software used in the current study [26] this procedure is termed "PC tuning."

In the OIM software, the software varies x*, y* and z* by a value $\pm 1\%$ from the starting position (x_0^*, y_0^*, z_0^*). (1% meaning 1% of the camera diameter in pixels). The pattern is indexed using a PC at each of the following 8 coordinates:

$$\begin{array}{ll} (x_0^* - 1\%, y_0^* - 1\%, z_0^* - 1\%) & (x_0^* + 1\%, y_0^* + 1\%, z_0^* + 1\%) \\ (x_0^* + 1\%, y_0^* - 1\%, z_0^* - 1\%) & (x_0^* - 1\%, y_0^* + 1\%, z_0^* + 1\%) \\ (x_0^* - 1\%, y_0^* + 1\%, z_0^* - 1\%) & (x_0^* + 1\%, y_0^* - 1\%, z_0^* + 1\%) \\ (x_0^* - 1\%, y_0^* - 1\%, z_0^* + 1\%) & (x_0^* + 1\%, y_0^* + 1\%, z_0^* - 1\%) \end{array}$$

which are essentially a set of vertices defining a box in PC space centered at the starting PC position. After indexing, the fit at each position is determined and the position producing the minimum fit identified. If the minimum fit at one of these points is less than that obtained at the starting position, then the procedure is repeated until the fit at the starting positions is less than that of all the points at the corners of the currounding box. The same procedure is repeated for a step size of 0.1% and again at 0.01%. For a 480x480 pixel pattern this is equivalent to about 0.05 pixels. However, this is not to claim that the accuracy of the PC method is less than a tenth of a pixel - but rather, simply the output of the algorithm. A recent study has shown that this approach gives good results for general orientation determination [4] but other work has shown that CC-EBSD measurements generally

require more accurate determination of the PC [39].

In the case of γ-TiAl and pseudosymmetry, this procedure needs to be performed three times with the starting orientation being set to each of the three pseudosymmetric solutions. In addition, the procedure is modified slightly so that during the iterative process of stepping through the different PC positions the orientations obtained after re-indexing remain near the original starting orientation, to ensure that the algorithm isn't switching from one pseudosymmetric orientation to another. After the PC tuning is performed for all three pseudosymmetric candidate orientations, the candidate producing the minimum fit value is assumed to be the correct solution [6] and that producing the best estimate of the PC.

2.4 Pattern Center Sensitivity

Pattern center error results in small relative shifts between the experimental pattern and the simulated reference pattern, introducing artificial strain and orientation error after cross-correlation. Since pseudosymmetric patterns are very similar, it is expected that pattern center error will have significant effect on the ability to resolve the correct orientation.

In order to determine the pattern center sensitivity of the five potential methods for resolving pseudosymmetry described in the previous section, the same simulated scan of γ-TiAl described in section 2.1 was used. Since the scan was simulated, the pattern center and orientation of each point were precisely known. The goal was to determine the maximum pattern center error that could be tolerated before the incorrectly identifying the pseudosymmetric orientation. This was identified by incrementally changing the expected pattern center of the "experimental" pattern relative to the actual pattern center used to generate the dynamically simulated pattern, thereby simulating increasing pattern center error. The five methodologies described

in section 2.2 were used to identify which of the three possible pseudosymmetric orientations most closely matched the experimental pattern. The result was then compared to the actual orientation used to generate the pattern and the number of incorrectly resolved points (out of the 100 points in the scan) was recorded.

2.5 Pattern Quality Sensitivity

Given the similarity of the patterns for pseudosymmetric orientations, it is expected that the quality of the EBSP will affect the ability of the cross-correlation and related image comparison methodologies described in section 2.2 will be dependent upon the quality of the patterns. A similar method to the one described in the previous section for determining pattern center error sensitivity was used to determine the sensitivity to pattern quality. Two metrics were used to quantify pattern quality: image resolution and Poisson noise.

The resolution of the images was incrementally reduced by simply binning the original patterns (1024 x 1024 resolution) as they were read into the algorithm. Poisson noise was introduced into the experimental patterns as they were read into the algorithm using the same method used by [40]. The noise and resolution were varied independently. The number of incorrectly resolved pseudosymmetries was identified for each level of binning and noise.

3 Results and Discussion

3.1 Simulated Scan

Pseudosymmetry in the simulated scan of γ-TiAl was successfully resolved using all 6 of the methodologies detailed in section 2.2. Figure 4 shows the IPF maps indicating the orientations of the simulated scan; the IPF color mapping is shown in Figure

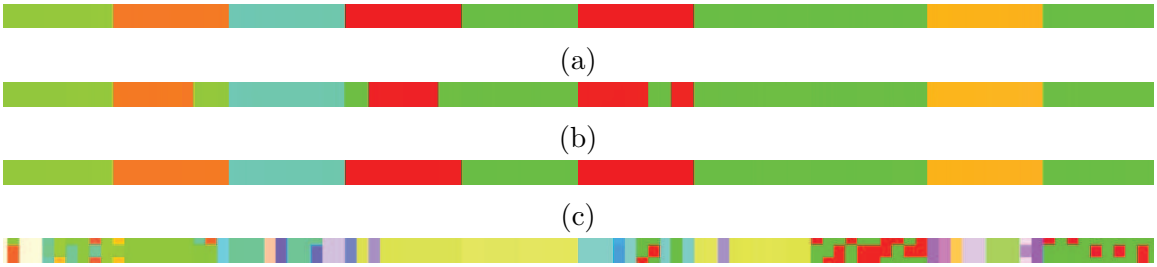

(a)

(b)

(c)

(d)

Figure 4: IPF maps of the simulated scans for the actual orientations of the simulated scan (a), orientations after indexing with OIM (b), orientations after correcting the indexed orientations using OpenXY (c), and orientations after indexing with OIM and a resolution reduction of 0.08 (d).

Figure 5: Legend for IPF maps generated by OIM, for the [001] direction.

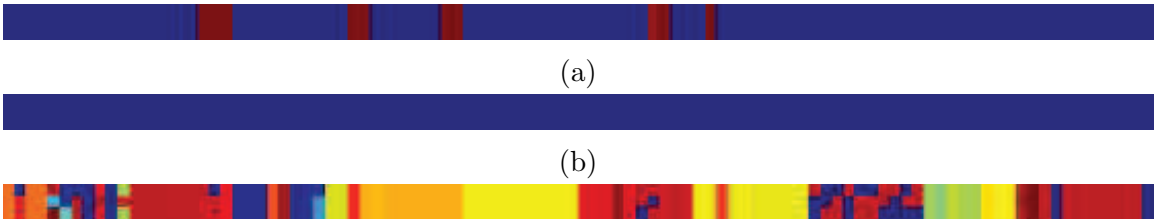

(a)

(b)

(c)

Figure 6: Misorientation maps of relative to the correct orientations after indexing with OIM (a), after correcting the indexed orientations using OpenXY (b), and after indexing with OIM with a resolution reduction of 0.08 (c).

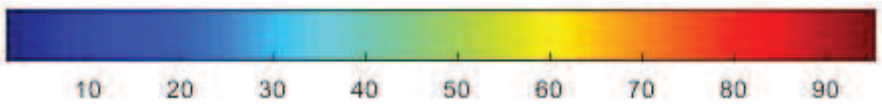

Figure 7: Color bar for misorientation maps

5. Figure 6 shows the misorientation of the simulated scan relative to the correct orientations; the misorientation color mapping is shown in Figure 7. Misorientations of approximately 90 degrees indicate the selection of an incorrect psuedosymmetric orientation.

After indexing the simulated patterns using OIM, 90% of the images were correctly indexed, as shown in Figures 4b and 6a. Each point of the scan was then analyzed with each of the 6 methodologies. Each methodology was 100% percent successful in identifying the correct orientation (see Figures 4c and 6b). Since all of the methodologies successfully resolved the psuedosymmetry where traditional Hough-based methods failed, and since the simulated patterns are ideal "perfect" patterns with excellent image quality and zero pattern-center error, further tests were performed to determine the relative advantages of each of the 6 methodologies by distorting simulated patterns.

Pattern Center Sensitivity

Figure 8 shows the sensitivity of the 6 methodologies to pattern center error. The sensitivity here is defined as the maximum error allowed before the method begins to mis-index the patterns. The results are also summarized in Table 2. The results were significantly different depending on the direction and the method. In general (with one exception), the pattern error should be kept lower than 0.4% of the pattern width in any direction. For the simulated patterns used in the study, this corresponds to about 4 pixels or 90 microns. The Z-direction was generally the most sensitive, and the smallest pattern center error that caused an incorrect pseudosymmetry to be selected was 0.06%, corresponding to an allowable error of 0.6 pixels or 13 microns. Previous studies have shown that current pattern center calibration methodologies can potentially correct the pattern center to within 0.01% of the pattern width (about 4 microns, or about one fifth of a pixel) [24], [41], and can therefore reduce the

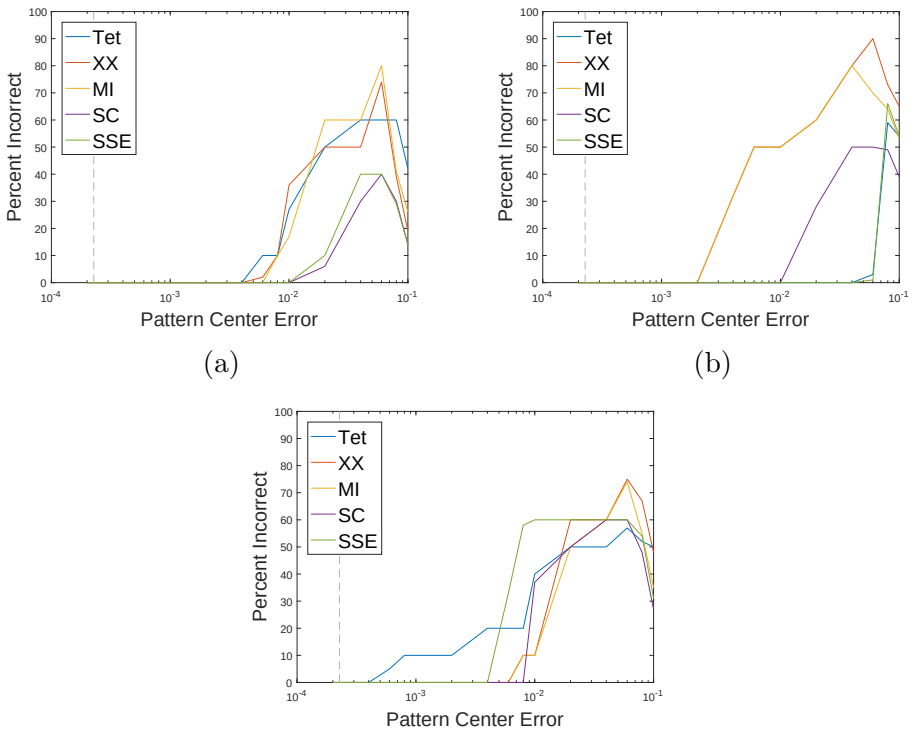

Figure 8: Pattern center sensitivity for the 6 methods for the x-direction (a), y-direction (b), and z-direction (c). Shows the percentage of patterns that are misindexed due to increasing pattern center error. Grey vertical bar shows typical resolution of pattern-center calibration techniques. Abbreviations in the legend are as follows: "Tet" = tetragonality, "XX" = cross-correlation coefficient, "MI" = mutual information, "SC" = shift confidence.

pattern center error to values within the sensitivity of any of the methodologies. The results for the experimental campaign of the current study matched the expected tetragonal behavior of pseudosymmetric grains, also indicating that the pattern center measurement is adequate.

Figure 9 shows the results from reducing the resolution of the pattern using standard binning techniques. The results show that most of the techniques are fairly robust to low resolutions: most of the techniques were able to successfully resolve images with a resolution as low as 82 x 82 pixels. At the same resolution, Hough-based indexing selected a pseudosymmetry for 36% of the patterns and accurately determined the orientation within 5 degrees for 16% of the patterns (see Figures 4d

Method	Pattern Center Sensitivity (In percent pattern width) X	Y	Z
Tetragonality	0.6	4.0	0.06
Cross-Correlation	0.6	0.4	0.8
Mutual Information	0.8	0.4	0.8
Shift Confidence	2.0	2.0	1.0
SSE	2.0	6.0	0.6

Table 2: Pattern center sensitivities for the five methods. Pattern center sensitivity is defined as the maximum pattern center error allowed before the method incorrectly identifies the true pseudosymmetric orientation. See caption for Figure 8 for definition of abbreviations.

and 6c). The results also show that using tetragonality is slightly more sensitive to resolution than other techniques (with the exception of SSE). This could result from the dependence of the technique on sub-sections of the image whereas mutual information and cross-correlation coefficients are holistic pattern comparisons and therefore use a larger percentage of the pixels. As the resolution reduces to about 20 x 20 pixels all methods fail between 50-60% of the time, which aligns fairly well with the expected purely random selection probability of 66%. Interestingly, as the resolution decreases to 10 x 10, the number of mis-indexed patterns for all methods decreases to about 30%.

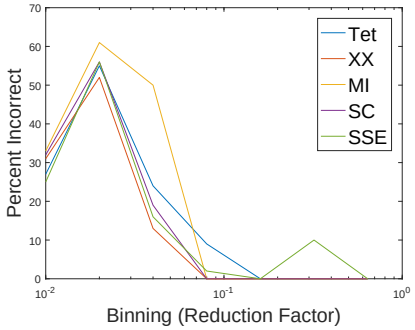

Figure 9: Sensitivity of the 6 methodologies to pattern resolution. Shows that most methodologies fail at a reduction factor of 0.08, which corresponds to a resolution of about 82 x 82 pixels and shown in Figure 10. See caption for Figure 8 for definition of abbreviations.

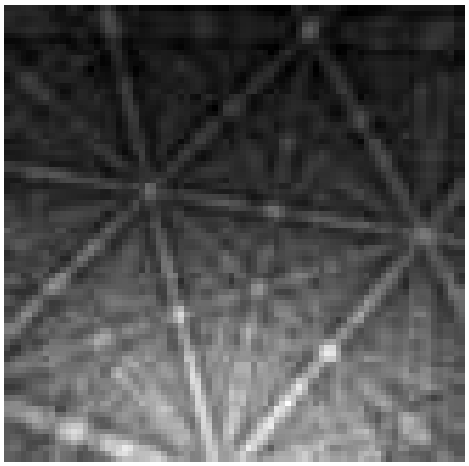

Figure 10: Lowest resolution pattern whose pseudosymmetry could successfully be resolved.

Sensitivity to Pattern Noise

Figure 11 shows the results from introducing Poisson noise into the simulated pattern using the poissrnd MATLAB function. All methods except using the SSE were able to resolve the pseudosymmetry up to significant levels of noise (see Figure 12). At the same level of Poisson noise shown in Figure 12 Hough-based indexed could not detect the bands and failed to index the patterns. This demonstrates that CC-EBSD techniques in general are robust to poor pattern quality. An ability to accommodate higher levels of noise allows for higher camera gains which allows for increased scan speed, reducing drift problems and cost.

Interestingly, for all three of the sensitivities evaluated in the current study (PC error, pattern resolution, and pattern noise) the effects showed a peak rather than a continually increasing or plateauing behavior. This could be due to artifacts within the CC-EBSD algorithm, where the patterns are so dissimilar that no reliable shifts are determined and the algorithm biases towards one particular solution, most likely the original solution.

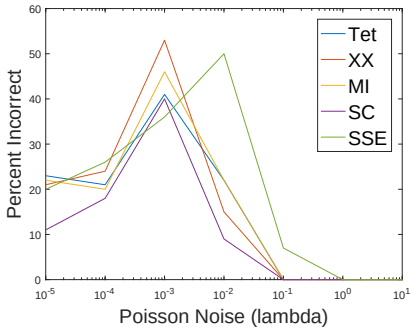

Figure 11: Sensitivity of the 6 methodologies to pattern noise. Shows that most methodologies fail when the noise increases above those shown in Figure 12. See caption for Figure 8 for definition of abbreviations.

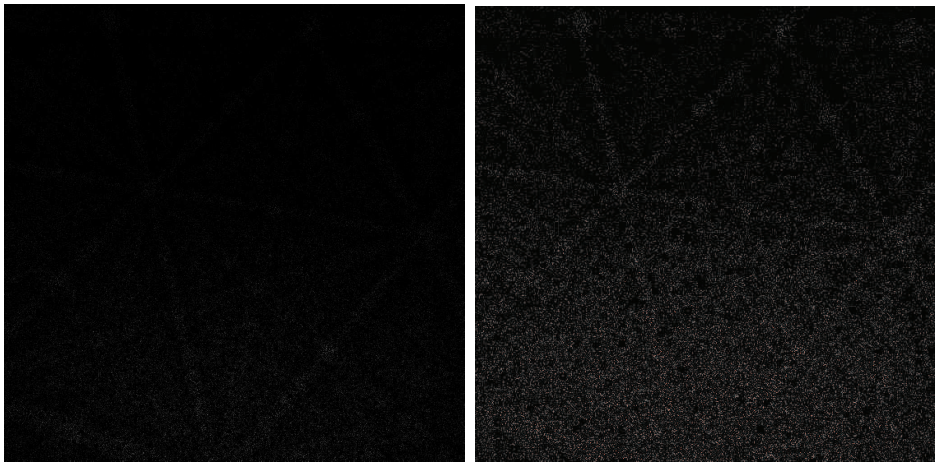

Figure 12: Maximum amount of Poisson noise before pseudosymmetry could not be resolved. The faint bands can barely be discerned in the unmodified pattern on the left. The brightness and contrast have been increased for the pattern on the right in order to make the noise of the pattern more easily discernible

3.2 Experimental Scan

In order to differentiate between the various methodologies for resolving pseudosymmetry, the methodology was tested on an experimental sample of γ-TiAl (described in 2.1). The pattern center was calibrated using the method described in Section 2.3 and was adjusted across the scan to account for the shift in pattern center with beam position. After pattern center calibration, each point in the scan was analyzed according to the methodology described in Section 2.2. Since the analysis evaluated all five methodologies for each point and was not optimized for computational effi-

ciency, the analysis took about 5 seconds per pattern on a Mac Mini™ with a 2.6 GHz Intel® Core™ i5 processor.

Figure 13 shows the IPF maps of the results for each of the 5 methods. Figure 14 shows the misorientation of each point with its neighbor in the negative-y direction (color mapping is given by Figure 7). Misorientations of about 90 degrees (points shown in red in Figure 14) are likely to be points that are incorrectly resolved pseudosymmetric orientations, since each of the three pseudosymmetric orientations have a relative misorientation of 90 degrees. Table 3 quantifies the potential accuracy of each method by calculating the percentage of points with misorientations less than 5°, between 5° and 85°, and greater than 85°, corresponding to points within the grain, noise or points at grain boundaries, or points that are pseudosymmetric orientations with their neighbor, respectively. Since the cross-correlation-based methods did not perform well in regions of poor image quality, a filter based upon Hough-based image quality from OIM was used to exclude regions of low image quality (see Figure 17) and the percentage was recalculated and included in the table. Values below about 75% of the maximum Hough-based image quality were filtered out. It should be noted that the actual number of incorrectly resolved points in the scan will be lower than the percentage given in Table 3, since one isolated incorrectly indexed point will cause two points to have a local misorientation of about 90 degrees (when considering misorientation in a single direction). Therefore, when 3% of the points have a local misorientation greater than 85 degrees suggests that between 3-1.5% of the points were incorrectly indexed. The results show that when considering all the points in the scan, none of the cross-correlation-based methods picked an orientation as consistently as OIM. However, when considering the regions of high image quality, which correspond to the areas of interest for the current study, all of the methods except SSE improved upon the original Hough-based results.

To more directly calculate the number of incorrectly indexed pseudosymmetric

points, a baseline orientation has to be selected. There are two predominant orientations in the lamellar structure, which will be denoted as "A" and "B," which correspond to the pink and green lamellae in the original IPF map, respectively (see labels in Figure 13a). For each lamellae "family," the orientation that was selected for more than half of the points was selected as the actual orientation for the lamellae. The percentage of points in each lamellae family that had a misorientation less than 85° with respect to the most common orientation is recorded in Table 4. The two lamellae families were identified by selecting a point in each family and then finding all the points in the scan that had a misorientation less than 5° with respect to that point, using a set of cubic instead of tetragonal symmetry operators. The "A" bands appear to have the most pseudosymmetry problems in the original IPF map (the creamy white color shown in Figure 13a).

	No Filter			With Filter		
Method	$< 5°$		$> 85°$	$< 5°$		$> 85°$
Original	83.6%	11.9%	4.5%	93.9%	1.7%	4.4%
Tetragonality	68.9%	23.7%	7.4%	93.7%	3.2%	3.1%
Cross-Correlation	67.9%	21.3%	10.8%	93.3%	2.7%	3.9%
Mutual Information	68.1%	20.9%	11.0%	93.7%	2.6%	3.7%
Shift Confidence	68.3%	23.8%	7.9%	94.8%	3.0%	2.2%
SSE	36.3%	22.5%	41.1%	50.6%	3.1%	46.5%
Hybrid	68.6%	20.6%	10.8%	94.2%	2.6%	3.3%

Table 3: Percent of points with a local misorientation (in degrees) with their neighbor in the -Y scan direction, divided by points with a misorientation less that 5 degrees, between 5 and 85 degrees, and greater than 85 degrees. Misorientations less than 5 degrees correspond to well-indexed points in the same grain, whereas misorientations between 5 and 85 degrees would correspond to grain boundaries or noise, and misorientations greater than 85 degrees correspond with points that are pseudosymmetric to each other. Therefore methods with a low percentage of points in the $> 85°$ window are desirable. The "With Filter" column reports the same statistic after scan points of low image quality have been removed.

	No Filter		With Filter	
Method	"A" Bands	"B" Bands	"A" Bands	"B" Bands
Original	96.9%	99.1%	96.1%	99.9%
Tetragonality	98.8%	87.2%	99.8%	90.8%
Cross-Correlation	98.4%	84.2%	99.8%	89.2%
Mutual Information	97.5%	90.5%	99.2%	94.5%
Shift Confidence	96.0%	93.6%	99.2%	98.0%
SSE	59.6%	75.2%	57.3%	72.6%
Hybrid	98.2%	90.5%	99.7%	94.5%

Table 4: Percent of points with a local misorientation less than 85 degrees with their neighbor in the -Y scan direction by lamellae family. The "With Filter" column reports the same statistic after scan points of low image quality have been removed. Lamellae family designation is shown in Figure 13a.

Tetragonality, Cross-Correlation Coefficient, and Mutual Information

As shown in Figures 13 and 14, the original map as indexed by OIM (Figure 13a) is very clean but lacks some of the clarity, especially of the thinner lamellae, shown in maps corresponding to tetragonality, cross-correlation coefficient, and mutual information approaches (Figures 13b, 13c, and 13d). Additionally, there are several lamellae with "noisy" orientations that indicate that the Hough-based indexing is switching between pseudosymmetric orientations (see the lamella with the label "A" in Figure 13a). Tetragonality, cross-correlation coefficient, and mutual information all performed exceptionally well in resolving the pseudosymmetry in the scan, and resolved about 99% of the points of high image quality in the "noisy" "A" lamellae, whereas the traditional Hough-based indexing picked a consistent pseudosymmetric orientation for about 96% (see Table 4). However, these methods did worse than the Hough-based methods in the "B" lamellae (89-95% for the cross-correlation methods vs 99.9% for the OIM results).

However, the cross-correlation-based methods selected a different pseudosymmetric orientation for the "B" bands. The tetragonality matched the predicted behavior

fairly well, where the true orientation has near-zero or positive tetragonality with the reference pattern, and the other two have negative tetragonalities of between 2-3%, and the cross-correlation coefficient and mutual information both had one value that was higher than two similar or nearly indentical value. Assuming that the cross-correlation method successfully identified the elongated c-axis by calculating the tetragonality and that therefore the orientations identified by tetragonality, cross-correlation coefficient, and mutual information are the correct orientations, the overall accuracy of each method is given in Table 5. Since the behavior of tetragonality, the cross-correlation coefficient, and the mutual information all matched that expected for pseudosymmetric patterns and selected the same orientation, identifying that orientation as the correct orientation is a fairly safe assumption. If this is the case, these three cross-correlation-based methods correctly indexed between 97-98% of the points of high image quality, compared to 74% for the Hough-based methods.

Shift Confidence

Shift confidence also performed well at consistently picking a particular orientation (as evidenced by the lack of random points within a grain with 90 degree misorientations from their neighbor) but picked a different orientation for the "A" lamellae than tetragonality, cross-correlation coefficient, and mutual information (see the change in the IPF maps in Figure 13 from green for maps (a-d) to blue in map (e)). This is likely because shift confidence is not a direct measure of correlation, like cross-correlation coefficient or mutual information, and instead is a measure of how well the convolution can determine a precise shift. It is possible that a combination of pattern center error and poor pattern quality contribute to a case where the shift is better defined for an incorrect pseudosymmetry. However, it is also possible that shift confidence is selecting the correct orientations while tetragonality, cross-correlation coefficient, and mutual information are not; from the previous section it was shown

that shift confidence is generally the least sensitive both to pattern center error and image quality. Without using more advanced validation techniques such as analysis with a TEM, it remains uncertain as to what the true orientation actually is. However, since tetragonality, cross-correlation coefficient, and mutual information all picked the same orientation and are more holistic and traditional methods of comparing patterns, it is most likely that they represent the true orientation.

SSE

The last potential measure of correlation between patterns, SSE, was clearly not effective at differentiating between the pseudosymmetric orientations as suggested by the very noisy IPF map shown in Figure 13f.

	No Filter			With Filter		
Method	Both	"A"	"B"	Both	"A"	"B"
Original	71.1%	96.9%	0.5%	74.2%	96.1%	0.0%
Tetragonality	95.7%	98.8%	87.2%	97.7%	99.8%	90.8%
Cross-Correlation	94.6%	98.4%	84.2%	97.4%	99.8%	89.2%
Mutual Information	95.6%	97.5%	90.5%	98.1%	99.2%	94.5%
Shift Confidence	27.2%	3.0%	93.6%	22.6%	0.3%	98.0%
SSE	19.9%	5.5%	59.4%	14.9%	1.2%	61.4%
Hybrid	96.1%	98.2%	90.5%	98.5%	99.7%	94.5%

Table 5: Percent of points that were correctly indexed, based upon the orientations determined using the detection of the c-axis using cross-correlation (i.e. tetragonality), by lamellae family. The "With Filter" column reports the same statistic after scan points of low image quality have been removed. Lamellae family designation is shown in Figure 13a.

Hybrid Method

Even though tetragonality, cross-correlation coefficient, and mutual information all picked the same orientations, none perfectly resolved the pseudosymmetry in all the lamellae. Of the three methodologies, mutual information performed the best at pick-

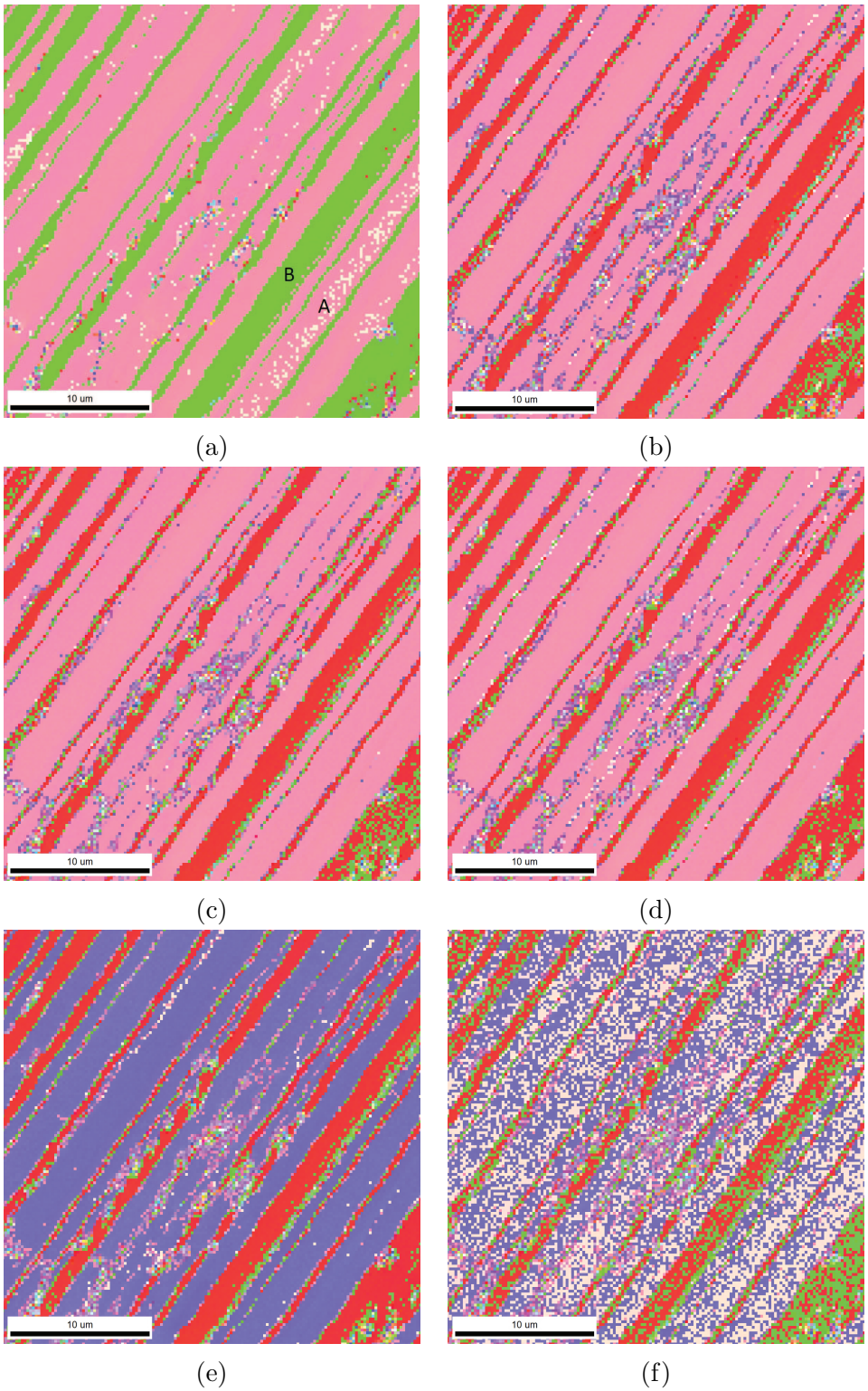

(a) (b) (c) (d) (e) (f)

Figure 13: IPF maps of the experimental scan for: original OIM orientations (a), and when the pseudosymmetry was resolved using tetragonality (b), normalized cross-correlation coefficient (c), mutual information (d), shift confidence (e), and SSE (f).

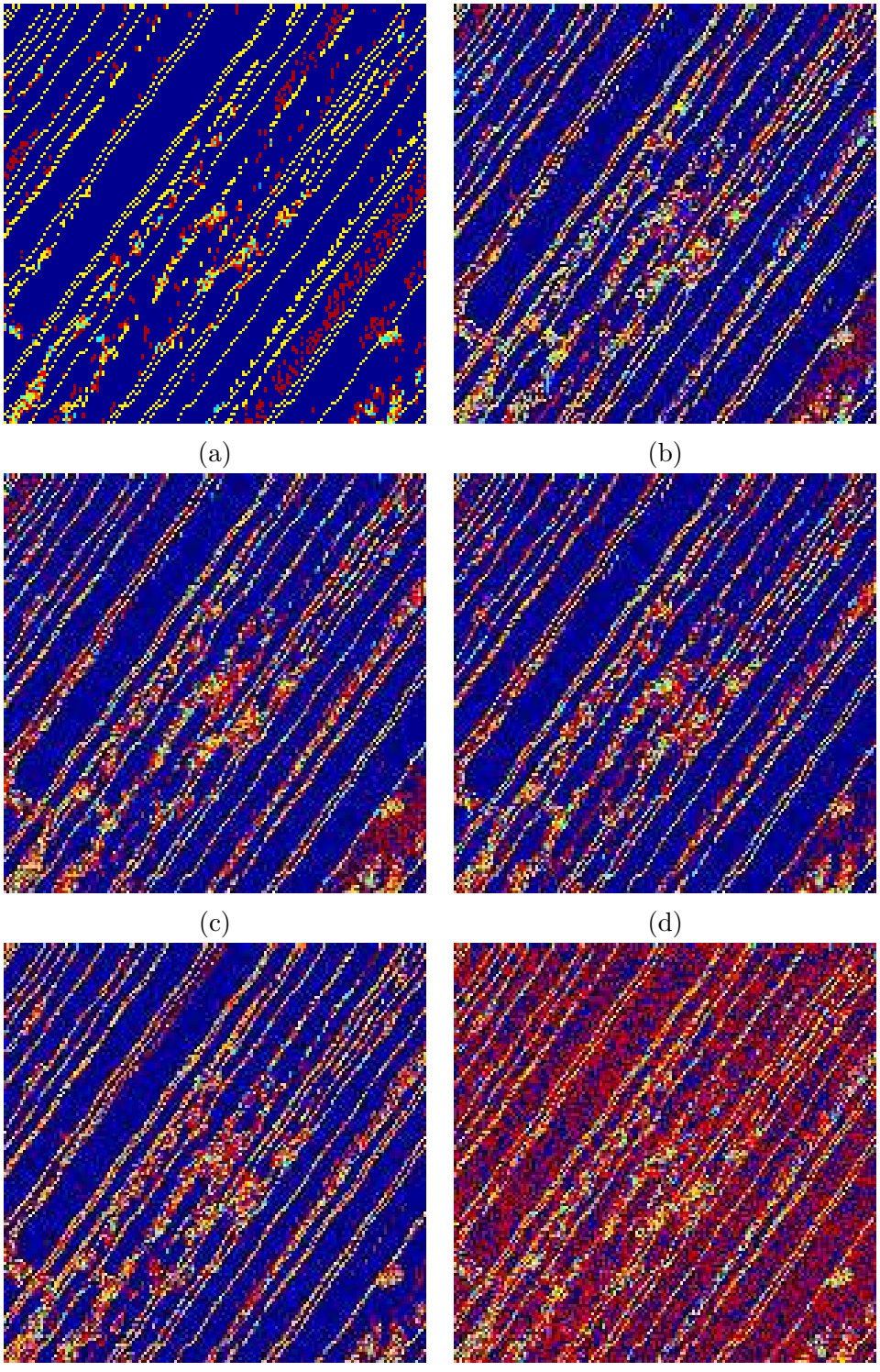

Figure 14: Misorientation maps of the experimental scan for: original OIM orientations (a), and when the pseudosymmetry was resolved using tetragonality (b), normalized cross-correlation coefficient (c), mutual information (d), shift confidence (e), and SSE (f).

Figure 15: Legend for IPF maps generated by OIM, for the [011] direction.

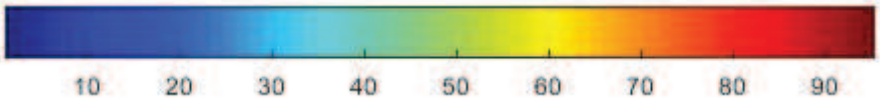

Figure 16: Color bar for misorientation maps

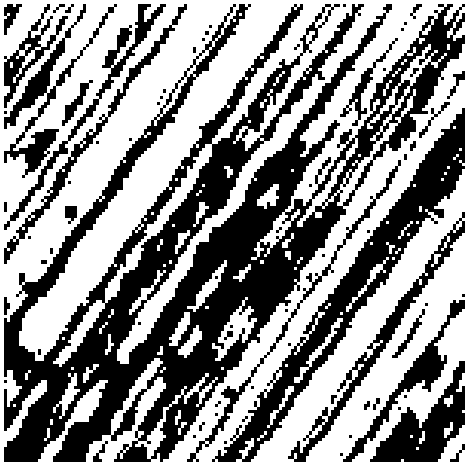

Figure 17: Plot of the filter overlay to exclude regions of low pattern quality. Black areas were excluded and white areas were included

ing a consistent orientation in the B lamellae, but performed slightly worse in the A lamellae. Therefore a "hybrid" method that systematically uses either tetragonality or the cross-correlation coefficient in high areas of confidence and mutual information as an alternative, could produce better results overall. The confidence of the resolution using the cross-correlation coefficient was quantified as the average separation of the cross-correlation coefficients, denoted XX_{sep}, and was calculated as follows:

$$XX_{max} = max(XX_{1,2,3}) \tag{6}$$

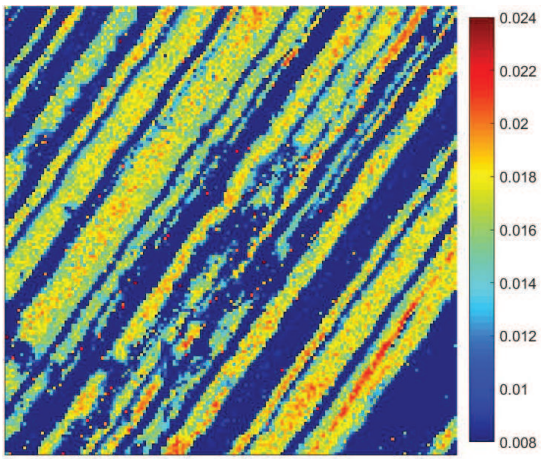

Figure 18: Plot of the separation between cross-correlation coefficients, defined as the average difference of the highest coefficient with the other two coefficients.

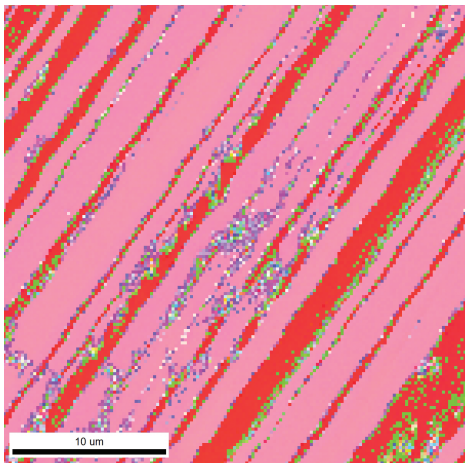

Figure 19: IPF map of the scan when resolved using a hybrid method using both tetragonality and cross-correlation coefficient

where $XX_{1,2,3}$ is a 3-element array of the cross-correlation coefficients of the pattern with each of the three pseudosymmetric reference patterns, and

$$XX_{mins} = (XX_{1,2,3} \neq XX_{max}) \tag{7}$$

where XX_{mins} is a two-element array of the coefficients that are not the maximum. The separation is therefore calculated as

$$XX_{sep} = \left| XX_{max} - \frac{\sum XX_{mins}}{2} \right| \tag{8}$$

A large value of XX_{sep} would therefore indicate a pattern was clearly better

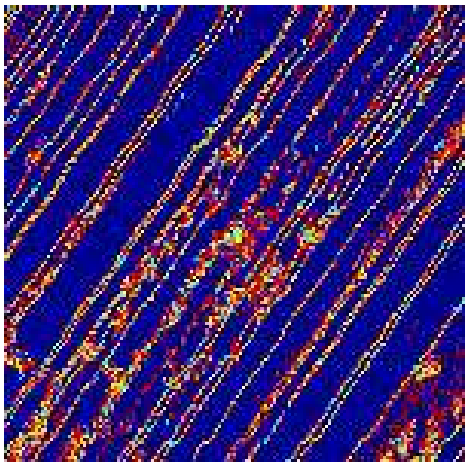

Figure 20: Misorientation map of the scan when resolved using a hybrid method using both tetragonality and cross-correlation coefficient

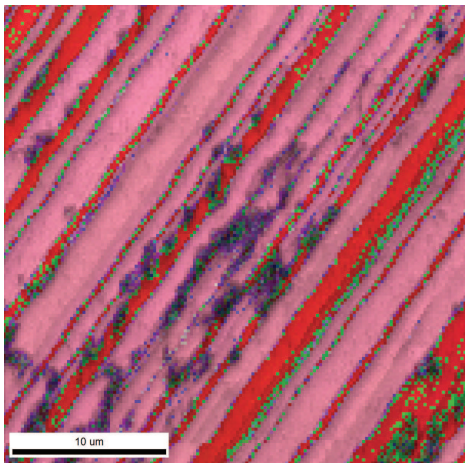

Figure 21: IPF map with grayscale image quality overlay of the scan when resolved using tetragonality. Shows that the poorly indexed regions correspond to regions of poor image quality.

correlated to the experimental pattern than the other two, whereas a small or near-zero difference would indicate an ambiguous selection between the three patterns. This difference was large in the central region of most of the "A" lamellae and low at the boundaries, and fairly low in the "B" lamellae (see Figure 18). A threshold value of 0.008 was selected above which the cross-correlation coefficient would be used to pick the correct pseudosymmetric orientation and below which the mutual information would be used to identify the correct orientation. The result is shown in Figures 19 and 20. As shown, overall this method cleans up the map better than

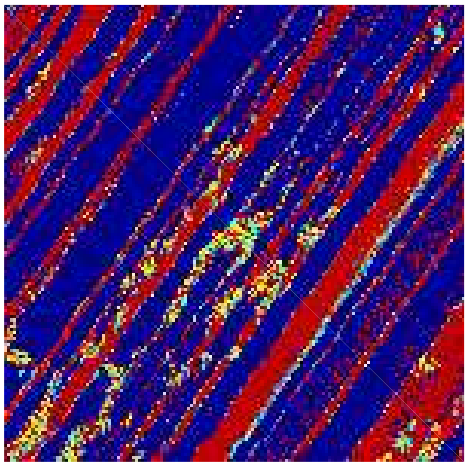

Figure 22: Misorientation map between the points in the scan as resolved by the hybrid method and the original orientations as indexed by OIM

either method individually. The areas that clearly do not resolve well correspond to areas of poor image quality, as shown in Figure 21, where the image quality overlays the IPF in grayscale. Figure 22 shows the misorientation of the results from the hybrid method relative to the original orientations as indexed by OIM and shows that most of the "B" lamellae were rotated by 90 degrees, indicating that OIM could have incorrectly indexed the large majority of the patterns in these areas, if they are in fact γ-TiAl.

It should be noted that there may be grains of hexagonal α_2-Ti_3Al, which does not exhibit pseudosymmetry. It is clear from the results that pseudosymmetry was very successfully resolved in the "A" lamellae (as high as 99.8% when using either tetragonality or the cross-correlation coefficient in areas of high image quality), but actually worsened the results provided by OIM in the "B" lamellae. It is possible that these "B" lamellae are in fact α_2-Ti_3Al, which would explain why the methods have difficulty consistently picking a single orientation when the "A" lamellae do not. If the crystal does not exhibit pseudosymmetry in these lamellae, it would randomly pick any of the three possible orientations; however, any bias such as pattern center error could cause it to pick one or two orientations more than another, as shown in

the results. It is also possible there is an orientational dependency to the algorithm where it perfoms better at some orientations than others, and without additional orientations it is impossible to address for the given experimental sample; however, the simulated patterns did not appear to show a strong orientational dependency. To resolve this ambiguity, the original scan was re-processed with OIM, allowing for the possibility of a hexagonal material. The B lamellae were not identified as hexagonal, which supports the results which demonstrate a tetragonal behavior in most of the B lamellae, with one value that stands out from two similar or nearly identical values. Therefore it is unlikely that the B lamellae are in fact α_2-Ti_3Al. While the cross-correlation methods didn't pick an orientation as consistently as OIM within the B lamellae, if the true orientation is in fact the one indicated by the cross-correlation methodologies, OIM erroneously picked the wrong orientation and the cross-correlation methodologies were fairly successful at correcting the results given by OIM. More definitive proof of the actual orientation requires more in-depth analysis of the sample using methodologies such as TEM analysis or detection of superlattice reflections, which lie outside the scope of the current study.

Overall, the results show that CC-EBSD can be used to effectively resolve pseudosymmetry in γ-TiAl, especially in the A lamellae. The hybrid approach discussed here that combines the relative merits of the cross-correlation coefficient and the mutual information may yield the best results; however, the shift confidence also performed exceptionally well and may benefit from further analysis as a potential metric for measuring the correlation between images. While the methodology performed well in the central regions of most of the bands, locations of poor image quality performed significantly worse than the Hough-based method, suggesting that the method may be more sensitive to poor pattern quality than suggested by the analysis using simulated patterns, and that the pattern quality metrics of pattern resolution and Poisson noise used in the current study do not completely capture the actual phenomena of

poor pattern quality.

Even though none of the methodologies were 100% successful at resolving the pseudosymmetry in the experimental sample, the hybrid methodology performed better than the Hough-based techniques used previously and cleaned up the orientations of the sample, uncovering microstructural information that was not readily apparent beforehand. This increased microstructural information may aid future research leading to better characterization of γ-TiAl.

4 Conclusion

The results successfully validated other studies showing that cross-correlation electron backscatter diffraction with dynamically simulated reference patterns can be used to resolve pseudosymmetry in materials with near-unity tetragonality, such as γ-TiAl. By analyzing simulated scans of γ-TiAl, the pseudosymmetry was successfully resolved for 100% of the scan for patterns free of pattern center error and at full resolution (1024x1024 pixels). The theoretical limits of the methodology were established and were found to be fairly robust to pattern center error, pattern resolution, and pattern noise, successfully resolving the pseudosymmetry for pattern center errors up to about 13 µm, pattern resolutions of 82x82 pixels, and Poisson noise with $\lambda = 0.1$. Subsequent studies could address the use of image processing to potentially mitigate the effects of noise.

The results of the analysis of an experimental sample of γ-TiAl demonstrated the capability of the methods set forth in this study to resolve pseudosymmetry in lamellar γ-TiAl, successfully indexing about 96% of the points in the scan. Of the several methodologies evaluated in this study—namely a calculation of tetragonality, the normalized cross-correlation coefficient, mutual information, shift confidence, and SSE of the cross-correlation—a hybrid method utilizing both the normalized cross-

correlation coefficient and the mutual information successfully resolved areas that Hough-based indexing methods failed to consistently index and revealed microstructure that was not immediately apparent before resolving the pseudosymmetry. The cross-correlation coefficient, the mutual information, and a measurement of tetragonality using CC-EBSD analysis all produced very similar results for the given sample. The study also demonstrated a new methodology for performing the pattern-center calibration to achieve very good results even with Hough-based indexing. While the Hough-based results for the current sample performed remarkably well at picking a consistent orientation, the cross-correlation methods suggest that they erroneously indexed one of the two sets of unique orientations within the sample, accounting for nearly 25% of the scan. Therefore, the results for the sample analyzed in the current study suggest that Hough-based methods may consistently pick a pseudosymmetric orientation, but cross-correlation methodologies should be used to more confidently identify the correct pseudosymmetric orientation in γ-TiAl.

The study showed that the cross-correlation coefficient and mutual information can be effectively used to consistently identify minute differences between patterns. The use of tetragonality calculations from CC-EBSD to resolve pseudosymmetry also illustrates the potential of CC-EBSD to measure absolute strain and therefore tetragonality. Shift confidence, a measure of the height of the convolution of sub-regions of the patterns, also performed exceptionally well and had excellent robustness to pattern center error, poor pattern resolution, and image noise. However, it picked a different pseudosymmetric orientation when resolving the pseudosymmetry in the experimental scan, compared to the cross-correlation coefficient, mutual information, and tetragonality. As a new measure of correlation proposed in this study, it may deserve further consideration and evaluation for its use within the CC-EBSD methodology. The SSE of the cross-correlation failed to resolve the pseudosymmetry in the experimental scan.

References

[1] B. Adams, S. Wright, and K. Kunze, "Orientation imaging: The emergence of a new microscopy," *Metallurgical and Materials Transactions*, vol. 24(4), pp. 8019–831, 1993.

[2] A. J. Schwartz, M. Kumar, B. L. Adams, and D. P. Field, *Electron Backscatter Diffraction in Material Science*. New York: Springer, 2009.

[3] S. I. Wright, M. M. Nowell, R. d. Kloe, and L. Chan, "Orientation precision of electron backscatter diffraction measurements near grain boundaries," *Microscopy and Microanalysis*, vol. 20, 2014.

[4] F. Ram, S. Zaefferer, T. Japel, and D. Raabe, "Error analysis of the crystal orientations and disorientations obtained by the classical electron backscatter diffraction technique," *Journal of Applied Crystallography*, vol. 48, 2015.

[5] S. I. Wright, J. A. Basinger, and M. M. Nowell, "Angular precision of automated electron backscatter diffraction measurements," *Materials Science Forum*, vol. 702, 2012.

[6] C. Zambaldi, S. Zaefferer, and S. I. Wright, "Characterization of order domains in γ-TiAl by orientation microscopy based on electron backscatter diffraction," *Appied Crystallography*, vol. 42, pp. 1092–1101, 2009.

[7] G. Nolze, A. Winkelmann, and A. P. Boyle, "Pattern matching approach to pseudosymmetry problems in electron backscatter diffraction," *Ultramicroscopy*, vol. 160, pp. 146–154, 2016.

[8] S. Dey, A. Morawiec, E. Bouzy, A. Hazotte, and J. Fundenberger, "A technique for determination of γ/γ interface relationships in a (α_2+γ) TiAl base alloy using TEM Kikuchi patterns," *Materials Letters*, vol. 60, pp. 646–650, 2006.

[9] S. Dey, E. Bouzy, and A. Hazotte, "EBSD characterization of massive γ nucleation and growth in a TiAl-based alloy," *Intermetallics*, vol. 14, pp. 444–449, 2006.

[10] B. Simkin, B. Ng, T. Bieler, M. Crimp, and D. Mason, "Orientation determination and defect analysis in the near-cubic intermetallic γ-TiAl using SACP, ECCI, and EBSD," *Intermetallics*, vol. 11, pp. 215–223, 2003.

[11] A. Sankaran, E. Bouzy, M. Humbert, and A. Hazotte, "Variant selection during nucleation and growth of γ-massive phase in TiAl-based intermetallic alloys," *Acta Materialia*, vol. 57, pp. 1230–1242, 2009.

[12] M. Vaudin, W. Osborn, L. Friedman, J. Gorham, V. Vartanian, and R. Cook, "Designing a standard for strain mapping: HR-EBSD analysis of SiGe thin film structures on Si," *Ultramicroscopy*, vol. 148, pp. 94–104, 2015.

[13] "EBSD analysis of TiAl alloys for texture and interphase boundary analysis," Oxford Instruments, Application Note.

[14] K. Troost, P. Sluis, and D. Gravesteijn, "Microscale elastic-strain determination by backscatter Kikuchi diffraction in the scanning electron microscope," *Appl. Phys. Lett.*, vol. 62, pp. 1110–1112, 1993.

[15] A. J. Wilkinson, G. Meaden, and D. J. Dingley, "High-resolution elastric strain measurement from electron backscatter diffraction patterns: New levels of sensitivity," *Ultramicroscopy*, vol. 106, pp. 301–313, 2006.

[16] J. Kacher, C. Landon, B. L. Adams, and D. Fullwood, "Bragg's Law diffraction simulations for electron backscatter diffraction analysis," *Ultramicroscopy*, vol. 109, pp. 1148–1156, 2009.

[17] T. Britton and A. J. Wilkinson, "High resolution electron backscatter diffraction measurements of elastic strain variations in the presence of larger lattice rotations," *Ultramicroscopy*, vol. 114, pp. 82–95, 2012.

[18] J. Alkorta, "Limits of simulation based high resolution EBSD," *Ultramicroscopy*, vol. 131, pp. 33–38, 2013.

[19] J. Kacher, J. Basinger, B. L. Adams, and D. T. Fullwood, "Reply to comment by Maurice et al. in response to "Bragg's Law Diffraction Simulations for Electron Backscatter Diffraction Analysis"," *Ultramicroscopy*, vol. 110, pp. 760–762, 2010.

[20] D. Fullwood, M. Vaudin, C. Daniels, T. Ruggles, and S. I. Wright, "Validation of kinematically simulated pattern HR-EBSD for measuring absolute strains and lattice tetragonality," *Materials Characterization*, vol. 107, pp. 270–277, 2015.

[21] P. Callahan and M. De Graef, "Dynamical EBSD patterns Part I: Pattern simulations," *Microscopy and MicroAnalysis*, vol. 19, pp. 1255–1265, 2013.

[22] A. Minkelmann, C. Trager-Cowan, F. Sweeney, A. P. Day, and P. Parbrook, "Many-beam dynamical simulation of electron backscatter diffraction patterns," *Ultramicroscopy*, vol. 107, 2007.

[23] A. Winkelmann, "Principles of depth-resolved Kikuchi pattern simulation for electron backscatter diffraction," *Journal of Microscopy*, vol. 239, pp. 32–45, 2010.

[24] B. Jackson, J. Christensen, S. Singh, M. De Graef, D. Fullwood, E. Homer, and R. Wagoner, "Performance of dynamically simulated reference patterns for Cross Correlation EBSD," *Microscopy and Microanalysis*, vol. 22, 2016.

[25] M. De Graef, *EMsoft 3.0*, 2015. [Online]. Available: `http://www.github.com/marcdegraef/EMSoft`.

[26] EDAX, *OIM Data Collection*, version 7.2.1, 2015.

[27] Brigham Young University, *OpenXY*, 2015. [Online]. Available: `https://github.com/BYU-MicrostructureOfMaterials/OpenXY`.

[28] A. Winkelmann, G. Nolze, and T. Lühur, "High-resolution EBSD pattern analysis for phase identification," in *EBSD 2014*, Pittsburgh, Jun. 17–19, 2014.

[29] E. Gulsoy, J. Simmons, and M. De Graef, "Application of joint histogram and mutual information to registration and data fusion problems in serial sectioning microstructure studies," *Scripta Materialia*, vol. 60, pp. 381–384, 2009.

[30] D. Dingley and K. Baba-Kishi, "Use of electron backscatter diffraction patterns for determination of crystal symmetry elements," *Scanning Electron Microscopy*, vol. 2, pp. 383–391, 1986.

[31] S. Biggin and D. Dingley, "A general method for locating the X-ray source point for Kossel diffraction," *J. Appl. Cryst.*, vol. 10, pp. 376–385, 1977.

[32] J. Venables and R. Bin-Jaya, "Accurate microcrystallography using electron back-scattering patterns," *Philosophical Magazine*, vol. 35(5), pp. 1317–1332, 1977.

[33] K. Mingard, A. Day, C. Maurice, and P. Quested, "Towards high accuracy calibration of electron backscatter diffraction systems," *Ultramicroscopy*, vol. 111(5), pp. 320–329, 2011.

[34] S. Wright, "Individual lattice orientation measurements development and application of a fully automatic technique," PhD thesis, Yale University, New Haven, 1992.

[35] J. Hjelen, R., E. Hoel, P. Runde, T. Furu, and E. Nes, "Ebsp, progress in technique and applications," *Texture, Stress, and Microstructure*, vol. 20(1-4), pp. 29–40, 1993.

[36] C. Maurice, K. Dzieciol, and R. Fortunier, "A method for accurate localisation of EBSD pattern centres," *Ultramicroscopy*, vol. 111, pp. 140–148, 2011.

[37] N. Krieger Lassen, "Source point calibration from an arbitrary electron backscattering pattern," *Journal of Microscopy*, vol. 195(3), pp. 204–2011, 1999.

[38] M. Nowell and S. Wright, "Phase differentiation via combined EBSD and XEDS," *Journal of Microscopy*, vol. 213(3), pp. 296–305, 2004.

[39] T. Britton, C. Maurice, R. Fortunier, J. Driver, A. Day, G. Meaden, D. Dingley, K. Mingard, and A. Wilkinson, "Factors affecting the accuracy of high resolution electron backscatter diffraction when using simulated patterns," *Ultramicroscopy*, vol. 110(12), pp. 1443–1453, 2010.

[40] L. Hansen, B. Jackson, D. Fullwood, S. I. Wright, M. De Graef, E. Homer, and R. Wagoner, "Influence of noise generating factors on Cross Correlation EBSD measurement of GNDs," *Microscopy and Microanalysis*,

[41] J. Basinger, D. Fullwood, J. Kacher, and B. Adams, "Pattern center determination in EBSD microscopy," *Microscopy and Microanalysis*, vol. 17, pp. 330–340, 2011.